PROCEEDINGS OF SCIENCE

Properties of New 50 cm Photodetectors in an Environment for Hyper-Kamiokande

Daisuke Fukuda[*a], **Yasuhiro Nishimura**[b], **Ryosuke Akutsu**[b], **Yusuke Suda**[c], **Miao Jiang**[d], **Seiko Hirota**[d], **Yuji Okajima**[e], **Yusuke Koshio**[a], **Masayuki Nakahata**[f], **Masato Shiozawa**[f], **Yoshinari Hayato**[f], **Shoei Nakayama**[f], **Hidekazu Tanaka**[f], **Masashi Yokoyama**[c], **Tsuyoshi Nakaya**[d], **Akimichi Taketa**[g], **Yoshihiko Kawai**[h], **Takayuki Ohmura**[h], **Masatoshi Suzuki**[h]

[a] *Department of Physics, Okayama University*
[b] *Institute for Cosmic Ray Research, University of Tokyo*
[c] *Department of Physics, University of Tokyo*
[d] *Department of Physics, Kyoto University*
[e] *Department of Physics, Tokyo Institute of Technology University*
[f] *Kamioka Observatory, Institute for Cosmic Ray Research, University of Tokyo*
[g] *Earthquake Research Institute, University of Tokyo*
[h] *Hamamatsu Photonics K.K.*

E-mail: fukudada@s.okayama-u.ac.jp

Hyper-Kamiokande is a next generation large water Cherenkov detector proposed for search for proton decay and neutrino observations. A 50cm Box-and-Line dynode photomultiplier tube (B&L PMT), which exhibits excellent time and energy resolution, was newly developed for Hyper-Kamiokande. The performance of the B&L PMT was confirmed under anticipated conditions in Hyper-Kamiokande such as expected magnetic field levels, high voltages and temperature ranges. Furthermore, the uniformity of timing and collection efficiency was measured for consistency with design. Characteristics of dark rate and afterpulse were also evaluated in detail.

International Conference on New Photo-detectors,PhotoDet2015
6-9 July 2015
Moscow, Troitsk,Russia

*Speaker.

PoS(PhotoDet2015)016

1. Introduction

The Hyper-Kamiokade (Hyper-K) is a next generation large water Cherenkov detector proposed for search for proton decay, neutrino observations and so on [1]. It consists of two tanks as shown in Figure 1, where each tank has dimensions of 48 m (W) $\times$ 54 m (H) $\times$ 250 m (L) . Its total (fiducial) volume is 0.99 (0.56) million tons, which is 20 (25) times larger than that of Super-Kamiokande. Hyper-K is designed for use with a 99,000-piece 50 cm photodetector system. Such photodetectors are required to have high resolution, low dark rate and low cost.

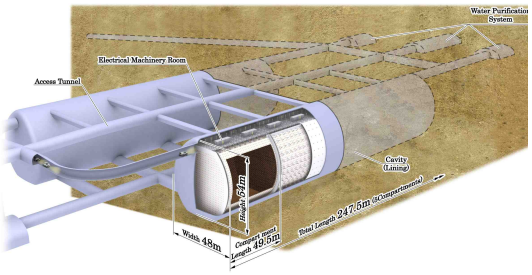

Figure 1: Hyper-Kamiokande detector.

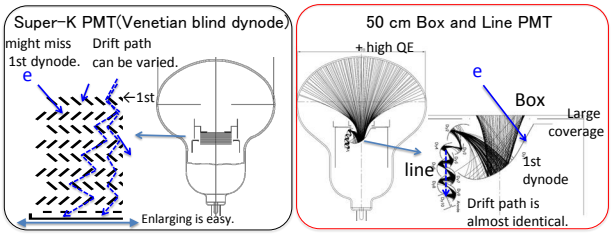

Figure 2: Left: SKPMT and principle of Venetian blind dynode; Right: Box-and-Line PMT and its principle.

2. Box-and-Line PMT

2.1 Design of Box-and-Line PMT

The 50 cm Box-and-Line dynode photomultiplier tube (R12860HQE, Hamamatsu Photonics K.K.) (B&L PMT) was developed for Hyper-K as one of the candidate photodetectors. Figure 2 shows the multiplier principles of B&L (right) and Venetian blind (left), where the latter is used for Super-Kamiokande as R3600, Hamamatsu Photonics K.K. (SKPMT) [2]. The B&L PMT has a large first dynode of "Box" shape and after second dynode of "Line" shape. "Box" maintains robust collection efficiency and "Line" demonstrates good timing resolution compared to that of the SKPMT. In addition, the newly developed phototube has a high quantum efficiency (HQE) photocathode that is 30% at peak wavelength, as opposed to 22% for the SKPMT typically.

2.2 Conditions of PMT usage in the Hyper-Kamiokande

Firstly, the Hyper-K uses coils to reduce geomagnetic fields as Super-Kamiokande does, with the residual magnetic field for the Hyper-K reaching at most a 100 mG level. Since the diameter of the PMT is quite large (50 cm), the residual geomagnetic field biases photoelectron trajectories in the PMTs. The effect of the magnetic field less than 100 mG has to be checked.

Secondly, high-voltage (HV) applied for each of the PMTs has a wide range (1,600 V to 2,200 V) for adjustment of gains. Such circumstances make arrival times and collection efficiencies (CEs) variable, because the electric field from the photocathode to the first dynode is changed for each HV. Thus, HV dependencies of the characteristics also have to be well known. Moreover, the water temperature in the Hyper-K is expected to be 13 °C while other disparate temperatures are actually maintained in the test measurement environment. Dark rates, in particular, demonstrate a strong dependency on temperature.

3. Uniformity of Box-and-Line PMT (photon incident position dependence)

Because of the large photosensitive area and the asymmetric shape of the B&L PMT dynode, timing and CE ultimately could depend on surface photon incident position. It would be important to measure the response so that Hyper-K could achieve the best performance with correcting the residual non-uniformity in the event reconstruction, after developing the B&L PMT with uniform response (as much as possible). The dependence on photon incident position was measured at typical HV without geomagnetism, compared with that affected by geomagnetic field and HV in an expected range in Hyper-K.

3.1 Measurement setup

The light from a laser diode is guided to a certain position on the surface of the PMT by an optical fiber. Figure 3 shows such a photon incident position. The X-axis is defined as the direction where the dynode is symmetrical, while the Y-axis is the direction where the dynode is asymmetrical. Figure 4 shows the setup of a Helmholtz coil, which can set the residual geomagnetic field similar to the Hyper-K condition. It can also apply an arbitrary magnetic and we can thus observe the magnetic field dependence of such characteristics. However, it has several error, which is $\pm$16 mG at center point of Helmholtz coil. The PMT was ultimately set inside this coil, with several measurements (via the application of different HVs) performed.

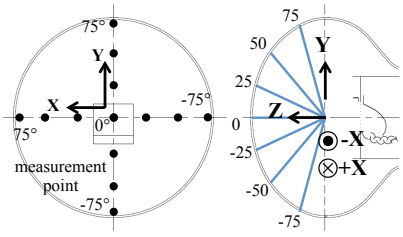

Figure 3: Definition of coordinate axes and incident point. Incident point is 0, 25, 50, 75 degrees of X and Y axes.

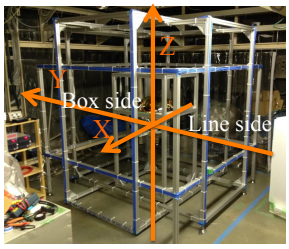

Figure 4: 3-D Helmholtz coil.

3.2 Timing differences

3.2.1 High voltage dependence

Thus, we measured the timing response of the B&L PMT with HV settings of 1,600, 1,800, 2,000, and 2,200 V in a reduced geomagnetic field condition less than $\pm$16 mG. Figures 5 and 6 show the transit time as a function of the photon incident position among several HV values. The transit time is defined as the timing which is a rising edge at 0.25 photoelectron. Here, the relative timing differences from measurements at the center position were determined because the timing offset as a function of HV can be easily calibrated as per the Hyper-K environment. However, the relative difference of the timing response is difficult to calibrate, which result in a deterioration of the vertex resolution.

As shown in the Figure 6, the timing of incident position at 75° is quite different with another position. This comes from the difference of the trajectory of photoelectrons which depends on the incident position. Especially in the edge of the PMT surface like 75°, the distance between

the hit position of the first dynode and the second dynode would be smaller than the case of the other position. Thus, the hit timing at this position becomes earlier. The timing response is slightly shifted by HV values, but the difference within 0.7 ns, that is variation shown by different colors in Figures 5 and 6, is negligible compared to the typical time resolution of 4.1 ns (FWHM).

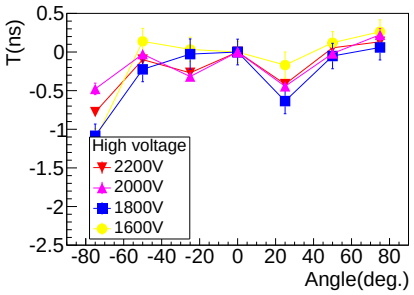

Figure 5: Difference of transit time by HV (scan for the X-axis).

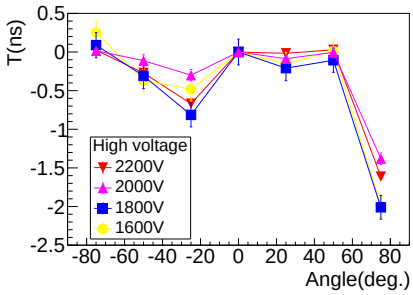

Figure 6: Difference of transit time by HV (scan for the Y-axis).

3.2.2 Magnetic field dependence

The trajectory of the photoelectron generated by photocathode also depends on the magnetic field. We measured the timing response at $\pm$100 mG along both axes. The associated experimental setup is similar to that described in Section 3.2.1, but a HV of 2,000 V is instead applied to the PMT; Figure 7 shows corresponding measured results. When a magnetic field was applied to the X-axis, a timing difference along the Y-axis was seen (upper-right in Figure 7). Likewise, when a magnetic field was applied to the Y-axis, a timing difference along the X-axis was seen (lower-left in Figure 7). This is the same reason as explained in the previous section, which comes from the difference of the trajectory of photoelectrons by the residual magnetic field. As a result, the point where the timing changed was only circumference of approximately 75°. Because this timing change was small compared to the timing resolution value, it does not affect the overall result.

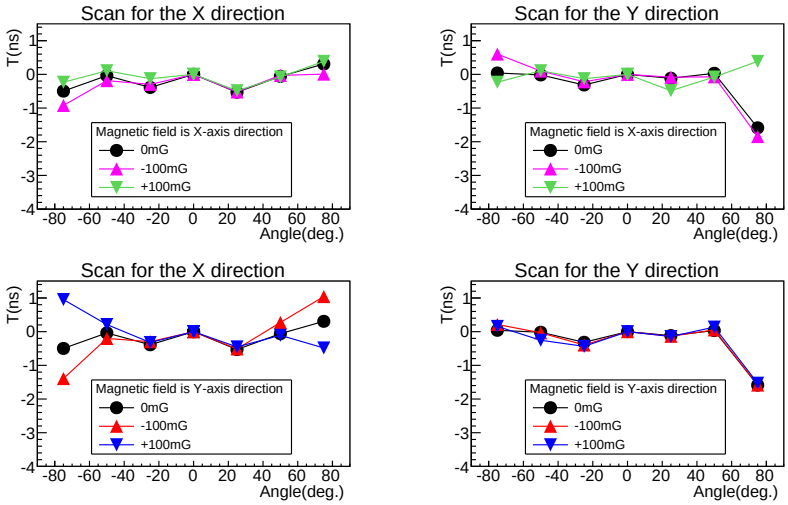

Figure 7: Uniformity of transit time in the magnetic field.

3.3 Relative collection efficiency

3.3.1 High voltage dependence

The CE of the B&L PMT amongst various HVs was measured in reduced geomagnetic field conditions. The CE is calculated by counting hits above 0.25 photoelectron in a low occupancy of the single photon injection. Figures 8 and 9 show relative CE values as a function of the photon incident angle for several HV values. The measurement setup is identical to that described in Section 3.2.1, with the associated data normalized by the value at 0°/ 2,000 V, which is defined as CE = 1 at 0°/ 2,000 V. As higher voltages were applied, better CEs were typically observed. Angle dependencies, however, were not evident, and no special efficiency drops emerged for any of the applied HV values as well.

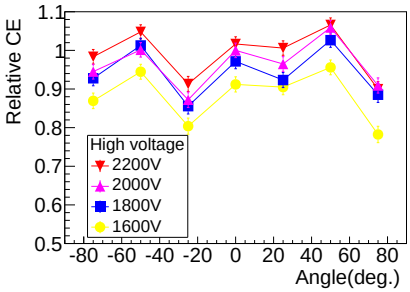

Figure 8: Difference of collection efficiency by HV (scan for the X-axis).

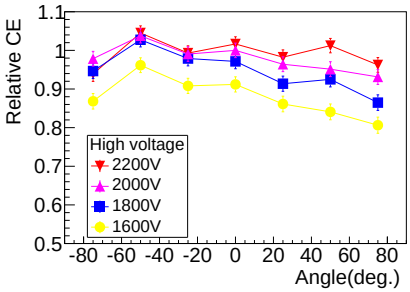

Figure 9: Difference of collection efficiency by HV (scan for the Y-axis).

3.3.2 Magnetic field dependence

Figure 10 shows the CE of PMT with different magnetic field intensities. The definition of CE for this case holds the same as that presented in Section 3.3.1. When a magnetic field is applied to the X-axis, a CE deficit along the Y-axis can be seen (upper-right in Figure 10). This is because of photoelectrons falling to different points or outside the dynode altogether via the magnetic field. It is expected as calculated by the design. However, the aforementioned decrease of CE appears only in the case in magnetic field of X-axis direction. Thus, it is possible to be avoided by considering the mounting direction at Hyper-K.

4. Temperature dependence of dark rate

The dark rate of the B&L PMT is currently around ten kilo hertz. Figures 11 and 12 illustrate the temperature dependency of dark rate. As higher HVs are applied, the dark rate is found to increase, with the temperature dependences varying with the HV as well. The dark rate was found to decrease approximately 30% from room temperature (22 °C) to the water temperature (13 °C) at 2,000 V, with an approximately 20% reduction seen at 1,800V.

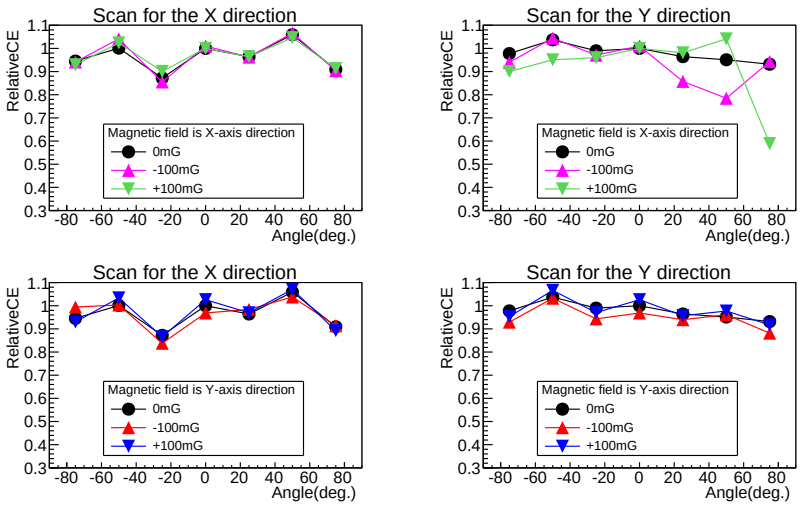

Figure 10: Uniformity of CE in magnetic fields.

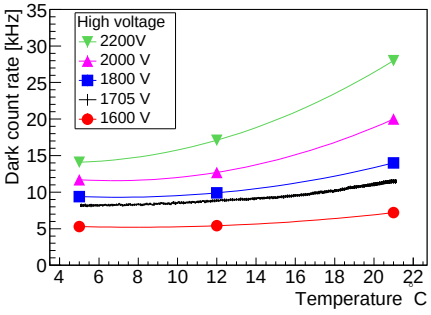

Figure 11: Dark rate as a function of each HV (1,600, 1,705 1,800, 2,000 and 2,200 V) with varied by temperature (5 °C to 21 °C), where 1,705 V (nominal gain) was continuously taken with changing the temperature.

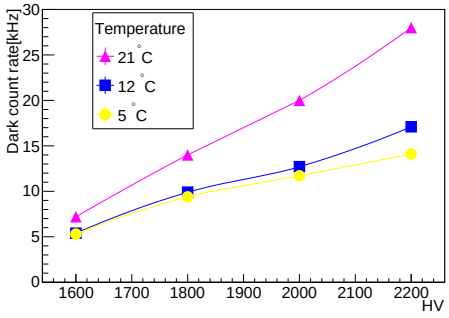

Figure 12: Dark rate as a function of each temperature (5 °C, 12 °C and 21 °C) with varied by each HV (1,600, 1,800, 2,000 and 2,200 V).

5. Afterpulse

An "afterpulse" occasionally accompanies a primary pulse signal [3]. When the primary pulse is amplified in the dynode, residual gases are ionized via interactions with electrons. Subsequently, the residual gas ions backtrack and ultimately emit electrons on the photocathode. These afterpulses are usually generated within approximately 50 μs after a primary pulse generation. It might be confused with decayed electrons from a muon decay in Hyper-K, for instance. Virtually all PMTs face difficulties associated with the afterpulse events. However, afterpulses with B&L dynodes can be particularly serious because of their large first dynode structures; thus, improvement in this regard was achieved by optimizing the dynode structure itself, as well as enhancing the man-

ufacturing process, dividing voltage rates, and so on. Afterpulse measurements were accordingly performed to confirm such sought-after reduced levels.

5.1 Results

Figure 13 shows the ratio of the expected value of the number of the afterpulses per 500 ns to the primary pulse, as a function of timing. Moreover, Table 1 shows the summary of afterpulse ratios for several B&L PMT models. The original ("old") B&L PMT has a large afterpulse rate, which is 32% of the primary pulse, while the new B&L PMTs (that employ afterpulse reduction initiatives) show small afterpulse rates, except for one (#EA0037). The reason why there are several different afterpulse rates (even in the latest versions) is that different production processes were attempted for optimization. The smallest afterpulse rate shows a comparable level to the SKPMT around 0.01 or less, therefore, it is concluded that afterpulses will not present any discernible issues in Hyper-K operation.

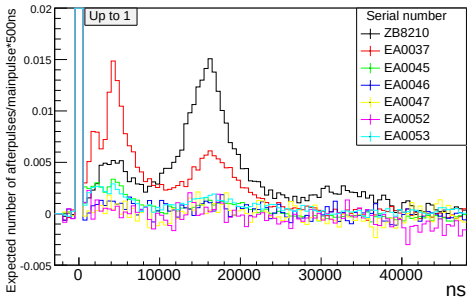

Figure 13: Time distribution of afterpulse.

Type	Serial number	Afterpulses / main pulse
Old	ZB8210	0.32 ± 0.03
New	EA0037	0.23 ± 0.04
New	EA0045	0.04 ± 0.02
New	EA0046	0.02 ± 0.01
New	EA0047	0.00 ± 0.02
New	EA0052	-0.02 ± 0.02
New	EA0053	0.07 ± 0.04

Table 1: Expected number of afterpulses / main pulse.

6. Summary

Photon incident angle dependencies of timing response and CE were measured amongst several magnetic field intensities and HV levels. The results were deemed in accordance with the anticipated characteristic environment of the Hyper-K. The only significant challenge of the initial prototype was afterpulse; however, the issue was solved in the newly developed version of the B&L PMT. As such, it was confirmed that the B&L PMT is ready for use in the Hyper-K.

References

[1] K. Abe *et al.* (The Hyper-Kamiokande working group) : Letter of Intent: The Hyper-Kamiokande Experiment Detector Design and Physics Potential, arXiv:1109.3262v1.

[2] A. Suzuki *et al.* : Improvement of 20 in. diameter photomultiplier tubes, Nucl. Instrum. Meth. A329 (1993) 299.

[3] K.J. Ma *et al.* :Time and Amplitude of Afterpulse Measured with a Large Size Photomultiplier Tube, arXiv:0911.5336.